

# Soft X-ray Polarization in Thermal Magnetar Emission

Matthew van Adelsberg<sup>1</sup> & Rosalba Perna<sup>2</sup>

<sup>1</sup>*Kavli Institute for Theoretical Physics, Kohn Hall, University of California, Santa Barbara, CA 93106*

<sup>2</sup>*JILA and Department of Astrophysical and Planetary Sciences, University of Colorado, Boulder, CO 80309*

20 November 2018

## ABSTRACT

Emission spectra from magnetars in the soft X-ray band likely contain a thermal component emerging directly from the neutron star surface. However, the lack of observed absorption-like features in quiescent spectra makes it difficult to directly constrain physical properties of the atmosphere. We argue that future X-ray polarization measurements represent a promising technique for directly constraining the magnetar magnetic field strength and geometry. We construct models of the observed polarization signal from a finite surface hotspot, using the latest NS atmosphere models for magnetic fields  $B = 4 \times 10^{13} - 5 \times 10^{14}$  G. Our calculations are strongly dependent on the NS magnetic field strength and geometry, and are more weakly dependent on the NS equation of state and atmosphere composition. We discuss how the complementary dependencies of phase-resolved spectroscopy and polarimetry might resolve degeneracies that currently hamper the determination of magnetar physical parameters using thermal models.

**Key words:** polarization – magnetic fields – radiative transfer – stars: atmospheres – stars: magnetic fields – stars: neutron – X-rays: stars.

## 1 INTRODUCTION

Thermal models of emission from neutron star (NS) surfaces and observations of NS cooling can be used to constrain the star equation of state (EOS), properties of matter at super-nuclear densities, and physics at extreme magnetic field strengths (e.g., Prakash et al. 2001; Yakovlev & Pethick 2004). Thermal radiation has been detected from several classes of isolated NSs, including Anomalous X-ray Pulsars (AXPs), Soft Gamma-ray Repeaters (SGRs), X-ray Dim Isolated Neutron Stars (XDINS; e.g., Haberl 2007), pulsars (e.g., Becker & Pavlov

2002; Marshall & Schulz 2002; De Luca et al. 2005), and central compact objects in supernova remnants (e.g., Sanwal et al. 2002; Mori et al. 2005; Kargaltsev et al. 2005). In this paper, we focus on emission from AXPs and SGRs, which comprise the population of magnetars, NSs that feature quiescent and bursting emission powered by the decay of strong interior magnetic fields with surface strengths  $B \sim 10^{14} - 10^{15}$  G (e.g., Woods & Thompson 2006, and the references therein). There is a near consensus in the literature that the magnetar hypothesis is correct. Evidence favoring the magnetar model includes the energetics, flux, and timing properties of SGR and AXP flares, long magnetar rotation periods and inferred ages, and the lack of sufficient NS rotational energy to power the observed quiescent emission (e.g., Kaspi 2004). This phenomenology is consistent with internal NS magnetic fields strengths of  $B \gtrsim 10^{15}$  G. However, other than the large magnetic dipole components calculated from timing measurements, there are no direct empirical constraints on external magnetar-strength magnetic fields. This is in part due to the lack of features in magnetar thermal spectra, a characteristic that is difficult to explain, since broad features have been observed in the spectra of NSs with lower magnetic fields and temperatures (e.g., XDINS and pulsars).

Moreover, differences between the observed characteristics of magnetars and other classes of high field NSs are still poorly understood. The recently discovered population of high-field radio pulsars is similar in most respects to canonical pulsars (they are powered by rotational kinetic energy and emit persistently in the radio band). However, the high-field radio pulsars have long periods and inferred magnetic field strengths of order  $B \gtrsim 4 \times 10^{13}$  G (e.g., Camilo et al. 2000; Gonzalez et al. 2004; Kaspi & McLaughlin 2005; Livingstone et al. 2006). Several authors have speculated that the distinct behaviors of magnetars and high field radio pulsars suggest differences in their magnetic field geometries and possible evolutionary connections between the two populations (e.g., Gonzalez et al. 2004).

One of the keys to understanding the nature of magnetars and their relationship to other NS populations is in the production of plausible theoretical models for interpreting observations. While significant progress has been made in modeling the spectra of thermal radiation from NS atmospheres, the use of such models to explain observational data is still in its infancy. In practice, typical soft X-ray magnetar spectra are fit equally well by blackbody or atmosphere models plus a power-law. The incorporation of vacuum polarization effects into NS atmosphere calculations has improved model fits to observed spectra, and has offered a possible explanation for the absence of magnetar spectral lines. In principle, predictions of

the beaming pattern of radiation along the surface magnetic field can be coupled to phase-resolved spectroscopy to discriminate between NS atmospheres and other emission models. However, the relatively low photon count rates from many magnetar sources, as well as the degeneracies between the NS magnetic configuration, viewing geometry, and compactness make it difficult to extract physical parameters from observations.

As an alternative, several recent works discuss the evolution of photon polarization states in NS magnetospheres, showing that, in the magnetar case, significant linear polarization fractions are expected, possibly containing a unique signature of the strong magnetic field (Heyl & Shaviv 2000, 2002; Heyl et al. 2003; Lai & Ho 2003a; van Adelsberg & Lai 2006; Wang & Lai 2009). Measurements of significant X-ray polarization, at 2.6 keV and 5.2 keV, were performed for the Crab nebula using the OSO-8 satellite (Weisskopf et al. 1976). These measurements confirmed an earlier detection by a sounding rocket experiment (Novick et al. 1972). However, as of this writing, no subsequent polarization measurements have been made for any object at energies  $E \sim 0.1 - 10$  keV (relevant for thermal magnetar emission). Recent advances in instrumentation have stimulated interest in future missions to perform polarimetry in the soft X-ray band, leading to several projects which are in active development (see Costa et al. 2001; Kallman 2004; Costa et al. 2006).

In this paper, we explore the future role of X-ray polarimetry as a complement to spectroscopy in interpreting observational spectra. We will argue that the combination of polarimetry and spectroscopy can constrain several critical NS parameters, including the temperature, magnetic field strength and geometry, size of emission region, and mass-to-radius ratio of highly magnetized NSs with  $B \sim 10^{12} - 10^{15}$  G. We use the latest magnetar atmosphere models of van Adelsberg & Lai (2006), and expand on the work of Heyl & Shaviv (2002), Heyl et al. (2003), Lai & Ho (2003a), and van Adelsberg & Lai (2006), to compute the phase-resolved, observed Stokes parameters from magnetars. We assume that these NSs have dipole magnetic field strengths of  $B = 4 \times 10^{13}$  G –  $5 \times 10^{14}$  G and emit from a region centered around the star polar cap with modest opening angle. We confirm that the polarization signal from a finite region on a magnetar surface retains important information about the strength of the magnetic field, as reported in previous works. We show that this signal has a strong dependence on the magnetic field and viewing geometry, and a weaker dependence on the NS EOS, emission region size, and atmosphere composition. Finally, we argue that polarization measurements can break the degeneracy inherent in inferring physical parameters from spectroscopic measurements alone.

Our paper is organized as follows: in §2, we discuss our assumptions and the atmosphere models used to calculate the emitted polarization fraction from the NS surface. In §3, we describe our methods for calculating the observed polarization signal from an extended NS polar cap, including relativistic effects. In §4, we show the results of our calculations for several representative cases. Lastly, in §5, we analyze our results, and compare and contrast the information obtained from polarization studies to that from phase-resolved spectroscopy.

## 2 PHYSICS INPUTS

In the canonical pulsar model, the magnetospheres of highly magnetized NSs contain tenuous plasma whose density is approximated by the Goldreich-Julian formula,  $n_{\text{GJ}} = fB/(ce) \approx 6.9 \times 10^{12} f_1 B_{14} \text{ cm}^{-3}$ , where  $f_1 = f/(1 \text{ Hz})$  and  $B_{14} = B/(10^{14} \text{ G})$  are the NS rotation frequency and magnetic field strength (e.g., Shapiro & Teukolsky 1986). The magnetar model contains a more complicated magnetic field structure compared to the standard dipole case. The presence of twisted magnetic fields (e.g., due to crustal motion and magnetic reconfiguration) leads to significant magnetospheric currents, which can, in principle, maintain electron-positron densities that are orders of magnitude larger than  $n_{\text{GJ}}$  (e.g., Thompson et al. 2002). This suggests the possibility that resonant cyclotron scattering in the magnetosphere distorts some of the radiation emerging from the NS surface, producing a NT component at energies  $E \sim 1 - 10 \text{ keV}$ . Modeling this emission requires sophisticated scattering calculations that depend on the magnetic geometry and magnetosphere structure; significant progress has been made in several recent works (Lyutikov & Gavriil 2006; Fernández & Thompson 2007; Rea et al. 2008).

In this paper, we focus on thermal photons that emerge directly from the NS surface, undistorted by scattering processes in the magnetosphere. In addition, we make the simplifying assumption that the NS has a pure dipole magnetic field. While the actual magnetar field structure is likely to be more complicated, it is unlikely to distort the polarization signal, which depends on the field structure at distances much greater than the star radius; far from the star, the field is dominated by the dipole component. If the emitted polarization is instead determined exclusively by processes at the NS surface or scattering, the vacuum polarization signature is destroyed.

In the work below, we assume that X-ray photons are emitted from a hot region with  $T_{\text{eff}} \sim 5 \times 10^6 \text{ K}$ , centered around the magnetic pole. The bulk emission from the rest of the

star is taken to be at a lower temperature and to contribute negligibly to the observed signal. We also assume that the size of the X-ray emission region is much smaller than the NS radius,  $R$ , with an approximately constant magnetic field normal to the NS surface. The opening angular radius of the polar cap is defined to be  $\beta < 2\pi$ . This geometry is consistent with what is observed in several magnetar sources. In quiescence and post-outburst, magnetars emit a thermal, soft X-ray component, with effective temperatures  $k_B T_{\text{eff}} \sim 0.3 - 0.5$  keV (along with a non-thermal, hard X-ray power-law). Single and two-component blackbody fits to observed, thermal X-ray spectra infer emission radii  $R_{\text{bb}} \lesssim 1$  km, implying that the radiation emerges from a small area (e.g., Tiengo et al. 2005; Israel et al. 2007).

Timing studies of AXPs and SGRs yield rotation periods of  $P \sim 10$  s, and imply dipole magnetic field strengths  $B \sim 10^{14} - 10^{15}$  G (e.g., Kulkarni et al. 2003; Mereghetti et al. 2005; Camilo et al. 2007; Israel et al. 2007).<sup>1</sup> van Adelsberg & Lai (2006) showed that, for  $P > 0.01$  s, calculations of the phase-resolved photon Stokes parameters are independent of rotation period.

In §2.1, we briefly discuss radiative transfer in magnetar atmospheres. In §2.2, we give a short review of the physics of vacuum polarization, and its effect on magnetar polarization.

## 2.1 Magnetar Atmosphere Models

Emission from magnetar surfaces is determined by radiative transfer through an atmosphere layer of ionized plasma (see Ho et al. 2003; van Adelsberg et al. 2005; Medin & Lai 2006, for cases in which these conditions may be violated). Due to gravitational setting, this atmosphere is likely to be composed of light elements, predominantly hydrogen or helium.

In a NS atmosphere, photons propagate in two polarization modes that have distinct interactions with the plasma medium. Ordinary (O) mode photons are linearly polarized, mostly in the plane formed by the photon propagation and magnetic field directions. They have an absorption opacity approximately equal to that of photons in non-magnetic plasma. Extraordinary (X) mode photons are linearly polarized mostly perpendicular to the plane formed by the propagation and magnetic field directions. They have an absorption opacity reduced by a factor  $(E_{Be}/E)^2$ , where  $E_{Be} \approx 1158B_{14}$  keV is the electron cyclotron energy, and  $E$  is the photon energy (e.g., Meszaros 1992). The reduction factor in the X mode

<sup>1</sup> For a complete, current reference list of magnetar observations and measured quantities, see <http://www.physics.mcgill.ca/~pulsar/magnetar/main.html>

absorption opacity is due to the suppression of particle motion transverse to the strong magnetic field, and is as large as  $10^6$  at photon energies  $E \sim 1$  keV. X mode photons therefore decouple from deeper layers of the atmosphere than O mode photons, and, under typical conditions, dominate the emergent radiation. Therefore, magnetar atmospheres emit strongly polarized radiation, with linear polarization fractions up to 100% (e.g., Pavlov et al. 1994; Ho & Lai 2003; Lai & Ho 2003b). In addition, atmospheric emission is beamed along the magnetic field, though the beaming pattern broadens when the effects of vacuum polarization in strong magnetic fields are taken into account (see van Adelsberg & Lai 2006, and the references therein).

The atmosphere models of van Adelsberg & Lai (2006) are the first to quantitatively incorporate the physics of vacuum polarization in strong magnetic fields, and produce accurate results for fully ionized atmospheres with field strengths  $B = 10^{12} - 10^{15}$  G. We use these radiative transfer calculations to construct the linear polarization fraction, defined:

$$\Pi_E^{\text{em}} = \frac{F_E^O(\delta) - F_E^X(\delta)}{F_E^O(\delta) + F_E^X(\delta)}, \quad (1)$$

where  $F_E^O(\delta)$  and  $F_E^X(\delta)$  are the observed intensities for X and O mode photons emerging from a hotspot on the star surface, and  $\delta$  is the angle between the photon propagation direction and surface normal (see §3.2).

## 2.2 Vacuum Polarization

When the NS magnetic field strength is greater than the quantum critical field  $B_Q \sim 4 \times 10^{13}$  G (obtained by setting the electron cyclotron energy equal to its rest energy), there are significant vacuum contributions to the dielectric tensor and magnetic permeability of the atmospheric plasma. At certain photon energies, propagation angles, and matter densities, plasma and vacuum contributions cancel each other out, leading to a vacuum “resonance” in which both photon modes become circularly polarized and the approximation of geometric optics breaks down (see Meszaros 1992; Lai & Ho 2002; Ho & Lai 2003, and the references therein). A photon of given energy  $E$ , propagating through the density gradient of the NS atmosphere, experiences two effects: (1) if it is X mode polarized, it experiences a significant enhancement of its absorption opacity in a narrow range of densities about the resonance; and (2) partial conversion occurs between X and O states in a manner analogous to the MSW effect for neutrinos (Lai & Ho 2002). The two primary effects of vacuum polarization on magnetar spectra are suppression of line features and softening of the hard tail present in

previous models (see, e.g., Ho & Lai 2001). For details on the physics of vacuum polarization and its effect on radiative transfer in magnetar atmospheres, see Lai & Ho (2002), Ho & Lai (2003), Lai & Ho (2003b), and van Adelsberg & Lai (2006).

It can be shown that photons of energy  $E$ , traveling through the vacuum resonance region, experience resonant mode conversion with probability  $P_C = 1 - \exp[-\pi(E/E_{\text{ad}})^3/2]$ . The adiabatic energy,  $E_{\text{ad}}$ , is defined:

$$E_{\text{ad}} \approx 2.52 \left[ f_B \tan \theta_B \left| 1 - (E_{Bi}/E)^2 \right| \right]^{2/3} H_\rho^{-1/3} \text{ keV}, \quad (2)$$

where  $\theta_B$  is the angle between the photon propagation direction and the magnetic field,  $H_\rho$  is the atmosphere scale height, and  $E_{Bi} \approx 0.63(Z/A)B_{14}$  keV is the ion cyclotron energy, with atomic and mass numbers  $Z$  and  $A$ , respectively. The parameter  $f_B$  is a slowly varying function of  $B$ , whose magnitude is of order unity. At photon energies  $E \ll E_{\text{ad}}$ , mode conversion is ineffective, while for  $E \gtrsim 1.4E_{\text{ad}}$ , mode conversion is essentially complete. The vacuum resonance density occurs at:

$$\rho_V \approx 0.96 (Z/A) E_1^2 B_{14}^2 f_B^{-2} \text{ g cm}^{-3}. \quad (3)$$

The vacuum resonance phenomenon leaves a unique signature on the emission of polarized radiation from the NS (Lai & Ho 2003a). For magnetic field strengths  $B \ll 7 \times 10^{13}$  G, photons of both modes encounter the vacuum resonance after decoupling from the NS atmosphere, while for  $7 \times 10^{13} \text{ G} < B < 5 \times 10^{16} \text{ G}$ , the vacuum resonance occurs at an atmospheric depth between the X and O mode photospheres (Lai & Ho 2003a). In the former case, photons encounter the vacuum resonance while propagating into the magnetosphere. For low energy photons with  $E \ll E_{\text{ad}}$ , mode conversion is ineffective, and the vacuum resonance has no effect on the emerging radiation. For high energy photons, mode conversion is effective, and results in conversion between the X and O polarization states. Thus, the vacuum polarization effect causes the plane of linear polarization to rotate  $90^\circ$  between low and high energies. This can occur in models with magnetic fields as high as  $B = 7 \times 10^{13}$  G, though there is a dependence on the NS geometry (see §4).

### 3 EMISSION MODEL

#### 3.1 Evolution of Photon Stokes Parameters in a Dipole Magnetosphere

After emerging from the atmosphere, photons propagate through the NS magnetosphere before reaching the observer. As discussed above, we ignore scattering and only consider magnetic field effects on the polarization mode evolution.

The solution to Maxwell’s equations in magnetized vacuum yields the unit polarization vectors for X and O mode photons in the magnetosphere (e.g., van Adelsberg & Lai 2006):

$$\hat{\mathbf{e}}_O = (\cos \varphi_B, \sin \varphi_B), \quad (4)$$

$$\hat{\mathbf{e}}_X = (-\sin \varphi_B, \cos \varphi_B), \quad (5)$$

where  $\varphi_B$  is the azimuthal angle of the magnetic field projected in a plane perpendicular to the observer line of sight (see below). Thus, the photon polarization state depends only on the magnetic field direction. The difference in the eigenvalues corresponding to the X and O polarization states is  $E\Delta n/(\hbar c) \sim 5 \times 10^3 E_1 B_{14}^2 (r/R)^{-6} \text{ cm}^{-1}$ , where  $E_1 = E/(1 \text{ keV})$  is the photon energy at the NS surface and  $r$  is the distance between the photon and the NS. When  $r \gtrsim R$ , the derivative of the angle for a dipole field is approximately  $d\varphi_B/ds \sim r^{-1} = 10^{-6} r_{10}^{-1} \text{ cm}^{-1}$ , where  $r_{10} = r/(10 \text{ km})$  and  $s$  is the affine parameter defined along the photon geodesic. Thus, near the star surface,  $E\Delta n/(\hbar c) \gg d\varphi_B/ds$ , and the polarization state evolves adiabatically with the changing direction of the magnetic field. As the photon continues to propagate in the magnetosphere, it reaches the polarization limiting radius,  $r_{\text{pl}}$ , where  $E\Delta n/(\hbar c) = d\varphi_B/ds$ . At distances greater than  $r_{\text{pl}}$ , the polarization state is fixed, and the directions of the mode vectors are constant. Thus, the measured values of the photon Stokes parameters are “frozen in” at  $r_{\text{pl}}$ . Far from the NS,  $d\varphi_B/ds \sim 1/r_l$ , where  $r_l \equiv c/\Omega$  is the light-cylinder radius. Therefore,  $r_{\text{pl}}$  takes the value:

$$r_{\text{pl}} \sim 1.5 \times 10^3 \left( E_1 B_{14}^2 f_1^{-1} \right)^{1/6} R_{10} \text{ km}. \quad (6)$$

In contrast, if the polarization states of emitted photons were determined near the NS surface, the observed signal would be greatly reduced. In this case, addition of the Stokes parameters for photons emitted from regions with distinct magnetic field directions would tend to cancel. Adiabatic evolution of the photon modes to distances far from the star surface, where the magnetic geometry is uniform, leads to significant polarization signals, even when emission occurs over an extended region on the star surface (Heyl & Shaviv 2002; Heyl et al. 2003).

We present calculations for NSs with a pure dipole magnetic field structure. As discussed above, realistic magnetar models include twisted magnetic field configurations which contain contributions from higher-order multipoles. Nevertheless, we have argued that because the polarization signal is fixed far from the star surface, the dipole component of the field is the most important for determining the observed Stokes parameters. Wang & Lai (2009) performed a detailed analysis of polarization mode evolution in a strongly magnetized vacuum, and showed that adiabaticity can be broken near the star surface only when the photon traverses a quasi-tangential region (where the photon direction is along the magnetic field). They presented a semi-analytic formalism for incorporating this effect into future calculations; however, for the polar cap sizes considered in this paper,  $\beta = 5 - 30^\circ$ , the correction will be small.

Lai & Ho (2003a) used the adiabaticity of photon mode evolution in the magnetosphere to develop a simple formalism for calculating the observed photon Stokes parameters. The results of their calculation are accurate for NSs with rotation periods  $P > 0.01$  s (van Adelsberg & Lai 2006). Following the work of Lai & Ho (2003a), we employ a fixed coordinate system,  $xyz$ , in which the observer line of sight is along the  $z$  axis. The rotation axis,  $\hat{\Omega}$  is defined to be in the  $xz$  plane, such that  $\hat{\Omega} \times \hat{z} = \sin \alpha_R \hat{y}$ , where  $\alpha_R$  is the angle between the rotation and  $z$  axes. The NS magnetic dipole moment vector,  $\boldsymbol{\mu}$ , is inclined at an angle  $\alpha_M$  relative to the rotation axis.

We define the rotational phase  $\psi$  as the azimuthal angle subtended by the magnetic dipole vector around the axis of rotation. The phase is taken to be  $\psi = 0$  when  $\hat{\boldsymbol{\mu}}$  is in the  $xz$  plane. The angle between  $\boldsymbol{\mu}$  and  $z$  is given by:

$$\cos \Theta = \cos \alpha_R \cos \alpha_M + \sin \alpha_R \sin \alpha_M \cos \psi. \quad (7)$$

The NS magnetic field, in the near-zone of the star such that  $r \ll \Omega/c$ , can be calculated according to the standard dipole formula,  $\mathbf{B} = [3(\boldsymbol{\mu} \cdot \hat{\mathbf{r}})\hat{\mathbf{r}} - \boldsymbol{\mu}] / r^3$ . Along the observer line of sight,  $r = z$ , and the projection of  $\mathbf{B}$  into the  $xy$  plane yields:

$$\cos \varphi_B = (\sin \alpha_R \cos \alpha_M - \cos \alpha_R \sin \alpha_M \cos \psi) / |\sin \Theta|, \quad (8)$$

$$\sin \varphi_B = -\sin \alpha_M \sin \psi / |\sin \Theta|. \quad (9)$$

Far from the NS, the photon geodesic is approximately  $\mathbf{r} \approx r\hat{\mathbf{z}}$ . The phase can be written  $\psi = \psi_{\text{em}} + r_{\text{pl}}/r_l$ , where  $\psi_{\text{em}}$  is the value of the rotational phase when the photon is emitted. For magnetars, which rotate slowly,  $r_{\text{pl}}/r_l \ll 1$ , and  $\psi \approx \psi_{\text{em}}$ .

For rapidly rotating NSs with  $f_1 \gtrsim 100$ , an accurate calculation of the observed polarization requires integration of the transfer equations for the photon Stokes parameters in the magnetosphere, which can result in significant circular polarization (van Adelsberg & Lai 2006). Circular polarization can also be generated in cases where the polarization limiting radius occurs close to either the NS surface or light cylinder radius (Heyl & Shaviv 2002). However, for magnetars with adiabatic evolution of the modes, the normalized Stokes parameters take the simple form:

$$Q_E/I_E = \Pi_E^{\text{em}} \cos(2\varphi_B), \quad (10)$$

$$U_E/I_E = \Pi_E^{\text{em}} \sin(2\varphi_B), \quad (11)$$

where  $I_E \equiv I_E^O(\theta_{\text{em}}) + I_E^X(\theta_{\text{em}})$  is the total specific intensity. The  $Q_E$ ,  $U_E$  Stokes parameters define the plane of polarization in the  $xyz$  coordinate system. Thus, measurements of the photon polarization directly map out the rotation of the magnetic dipole field around the NS.

### 3.2 Emission from a Finite Spot

Phase-dependent emission from an extended area on a NS surface is computed according to the method described by Pechenick et al. (1983), using the generalizations of Perna & Gotthelf (2008). We assume that the radiation emerges from a single spot, centered around the magnetic dipole vector, with opening angle  $\beta$ . Thus, the angle between the spot center and observer line of sight is given by equation (7). We describe points on the NS surface using the polar angle  $\theta$  and azimuthal angle  $\varphi$ , in spherical polar coordinates. If  $\Theta = 0$ ,  $\theta$  is restricted to  $\theta \leq \beta$ , otherwise the condition becomes:

$$\Theta - \beta \leq \theta \leq \Theta + \beta \quad (12)$$

$$2\pi - \varphi_\star \leq \varphi \leq \varphi_\star, \quad (13)$$

where

$$\cos \varphi_\star = \frac{\cos \beta - \cos \Theta \cos \theta}{\sin \Theta \sin \theta}. \quad (14)$$

When  $0 < \Theta < \beta$ , the constraints on  $\theta$  and  $\varphi$  become:

$$\theta \leq \theta_\star(\Theta, \varphi, \beta), \quad (15)$$

$$\cos \beta = \sin \Theta \sin \theta_\star \cos \varphi + \cos \Theta \cos \theta_\star, \quad (16)$$

where equation (16) must be solved numerically. The values of  $\theta$  and  $\varphi$  that describe points in the spot are restricted to those that yield solutions for co-angles  $\varphi_*(\beta, \Theta, \theta)$  or  $\theta_*(\beta, \Theta, \varphi)$ , depending on the conditions.

Due to general relativistic effects, a photon emitted from colatitude  $\theta$  will reach the observer if emitted at an angle  $\delta$  with respect to the surface normal, where the relation between the two angles is given by the ray-tracing function (Pechenick et al. 1983; Page 1995):

$$\theta(\delta) = \int_0^{R_s/2R} du x \left[ \left(1 - \frac{R_s}{R}\right) \left(\frac{R_s}{2R}\right)^2 - (1 - 2u)u^2x^2 \right]^{-1/2}. \quad (17)$$

In equation (17),  $x \equiv \sin \delta$ ,  $R_s \equiv 2GM/c^2$  is the Schwarzschild radius, and  $M$  is the NS mass. In our calculations, we assume that  $M = 1.4M_\odot$  and  $R = 12$  km. A simpler, more convenient relationship between the emission angle and colatitude is given by the approximation in Beloborodov (2002):

$$\cos \delta \approx \frac{R_s}{R} + \left(1 - \frac{R_s}{R}\right) \cos \theta. \quad (18)$$

Equation (18) differs from (17) by less than 1% when  $R > 3R_s$ . The portion of the NS surface visible to the observer is given by the set of  $\theta$  values that yield solutions for  $\delta$  in equation (18).

The total, phase-dependent specific intensities from the spot are then obtained by integrating the local emission in each mode over the observable surface, accounting for the gravitational redshift of the radiation (Page 1995):

$$F^j(E_\infty, \psi) = \int_0^1 dx x \int_0^{2\pi} d\varphi I_j(\theta, \varphi, E_\infty e^{-\Lambda}), \quad (19)$$

where the local specific intensity in each mode  $I_j$  ( $j = X, O$ ) is set to zero outside of the boundaries on  $\theta$  and  $\varphi$  set above. The energy observed at infinity is given by  $E_\infty = Ee^\Lambda$ , with

$$e^\Lambda = \sqrt{1 - \frac{R_s}{R}}. \quad (20)$$

The phase-dependent Stokes parameters are then readily calculated using the methods of §3.1.

## 4 RESULTS

We present results from our magnetar models with fully ionized hydrogen atmospheres, magnetic field strengths  $7 \times 10^{13}$  G –  $5 \times 10^{14}$  G, and effective temperature  $T_{\text{eff}} = 5 \times 10^6$  K

(a value which is in the typical magnetar range). We explore four representative geometries:  $\alpha_R = 90^\circ$ ,  $\alpha_M = 90^\circ$  (hereafter denoted G1);  $\alpha_R = 90^\circ$ ,  $\alpha_M = 45^\circ$  (hereafter denoted G2);  $\alpha_R = 45^\circ$ ,  $\alpha_M = 45^\circ$  (hereafter denoted G3); and  $\alpha_R = 45^\circ$ ,  $\alpha_M = 0^\circ$  (hereafter denoted G4).

#### 4.1 Atmosphere Model Linear Polarization Fractions

As discussed above, quiescent magnetar emission spectra are well fit by a blackbody plus power-law and do not contain absorption features. Thus, it is difficult to distinguish magnetic atmosphere models from phenomenological fits. However, the linear polarization is strongly dependent on the magnetic field and viewing geometry, and, importantly, cannot be predicted without a detailed physical model for the surface emission. In this section, we describe the dependence of  $\Pi_{\text{em}}$  on magnetic field and geometry.

Figures 1 and 2 show the linear polarization fraction calculated using NS atmosphere models at magnetic field strengths  $B = 5 \times 10^{14}$  G (solid curves),  $B = 10^{14}$  G (dotted curves), and  $B = 7 \times 10^{13}$  G (dashed curves). Each panel in the figure corresponds to one of the NS geometries described above. The polar cap size is set to  $\beta = 5^\circ$ .

Figure 1 shows results for photons with energy  $E = 0.5$  keV. The upper-left panel depicts the case of the “orthogonal rotator,” in which the magnetic dipole vector rotates in the  $yz$  plane, intersecting the line of sight at  $\psi = 0$ . The upper-right and lower-left panels show less extreme geometries. In G2, most of the photons are emitted with  $\delta \gtrsim \pi/4$ , and in G3, the dipole vector intersects the line of sight when  $\psi = 0$ , but sweeps out a cone whose base is perpendicular to the NS rotation axis. The lower-right panel shows the extreme case when the rotational and magnetic axes are aligned.

There are two key features of Figure 1 that highlight the interplay between the NS geometry, magnetic field strength, and vacuum polarization effects to produce the emitted polarization. These features include: (1)  $|\Pi^{\text{em}}|$  is smaller for values of  $\psi$  close to 0 than for values of  $\psi$  close to  $\pi/2$ ; (2) at  $\psi \approx 0$ , the sign of  $\Pi^{\text{em}}$  is positive for  $B = 7 \times 10^{13}$  G, and negative for stronger magnetic fields.

Result (1) can be understood by considering the variation in X and O mode opacities with angle between the photon propagation and magnetic field directions. For the orthogonal rotator, small phases roughly correspond to emission along the observer line of sight and magnetic field direction. For emission angles  $0 < \delta \ll 2\pi$ , the difference between the free-

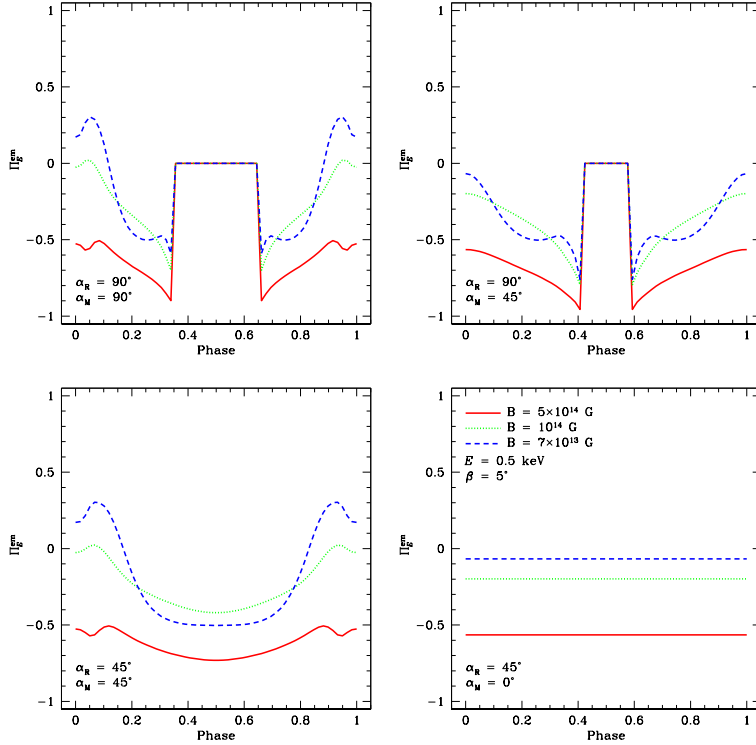


**Figure 1.** Emitted polarization fraction,  $\Pi_E^{\text{em}} \equiv (I_O - I_X)/(I_O + I_X)$ , as a function of phase, for an extended spot on a NS surface. The spot is located at the magnetic pole and has opening angle  $\beta = 5^\circ$ . Results are shown for four NS geometries and three magnetic field strengths:  $B = 5 \times 10^{14}$  G (solid curve),  $B = 10^{14}$  G (dotted curve), and  $B = 7 \times 10^{13}$  G (dashed curve). The angles  $\alpha_R$  and  $\alpha_M$  are the polar inclinations of the rotation axis relative to the line of sight, and the magnetic dipole vector relative to the rotation axis, respectively. The photon energy is set to  $E = 0.5$  keV.

free absorption opacities of the X and O modes is smaller than for angles  $\delta \approx \pi/4$  (see §2.6 of Ho & Lai 2001). The densities at which X and O mode photons decouple from the atmosphere are therefore closer in value, leading to the smaller magnitude of  $\Pi^{\text{em}}$ . Conversely, at phases for which  $\psi \gtrsim \pi/2$ , emission angles for photons reaching the observer are  $\delta \lesssim \pi/4$ . At these angles, the difference between the X and O mode opacities (and hence, decoupling depths) is maximal, yielding larger values of  $|\Pi^{\text{em}}|$ . This trend is also visible in geometries G2 and G3 of Figure 1, where in the G3 case, emission angles  $\delta \approx \pi/4$  are realized for phases  $\psi \approx \pi$ . In the G4 geometry, the emission angle and hence the polarization are independent of the phase.

Result (2) is a manifestation of the vacuum polarization effect. As discussed above, for typical angles and photon energies, the emitted specific intensity of X mode photons is greater than that of O mode photons. Under these conditions,  $\Pi^{\text{em}} < 0$ . However, at magnetic field strength  $B = 7 \times 10^{13}$  G, photons with energy  $E = 0.5$  keV encounter the vacuum resonance at a density  $\rho_V \lesssim \rho_O$ , where  $\rho_O$  denotes the O mode decoupling density. Thus, if resonant mode conversion occurs,  $\Pi^{\text{em}}$  will switch sign, corresponding to a rotation of

the plane of linear polarization. At emission angles  $\delta \approx \pi/4$  and photon energies  $E = 0.5$  keV, the mode conversion probability is much less than unity. However, when the emission angle  $\delta \approx 0$ , the mode evolution becomes adiabatic, and  $P_C \rightarrow 1$ . Therefore, at phases for which the emission angle is small, resonant mode conversion occurs and the sign of  $\Pi^{\text{em}}$  changes. For magnetic fields  $B > 10^{14}$  G, the vacuum resonance density is intermediate between the X and O mode decoupling densities, and no change in the plane of linear polarization occurs. Rotation of the plane of linear polarization at  $B < 7 \times 10^{13}$  G occurs in geometries G1 and G3 (upper- and lower-left panels), in which  $\psi \rightarrow 0$  corresponds to  $\delta \rightarrow 0$ . In geometries G2 and G4, (upper- and lower-right panels), the emission occurs at angles  $\delta \approx \pi/4$ , resulting in little mode conversion at  $E = 0.5$  keV.

As the magnetic field strength is increased, the suppression factor in the X mode free-free absorption opacity increases as  $B_{14}^2$ . Thus, we expect the emitted polarization fraction to increase (roughly) with the strength of the atmosphere magnetic field. When vacuum effects are taken into account, the decoupling depth of X mode photons is effectively reduced by the increase in free-free absorption opacity and mode conversion at the resonance (Ho & Lai 2003). If the X mode photon decoupling density is approximately equal to the vacuum resonance density, the trend is preserved ( $\rho_V \propto B_{14}^2$ ). This results in large values of  $|\Pi^{\text{em}}|$  at  $B = 5 \times 10^{14}$  G relative to those at  $B = 7 \times 10^{13}$  G.

Figure 2 shows the same results as figure 1, except for photons with  $E = 2$  keV. While the general variation in  $|\Pi^{\text{em}}|$  with phase remains the same as in the  $E = 0.5$  keV case, the rotation of the plane of polarization at  $\psi \approx 0$  no longer occurs. This is because, at  $B = 7 \times 10^{13}$  G, photons with  $E = 2$  keV encounter the vacuum resonance at a larger density, which occurs between the X and O mode photospheres for  $\delta \ll 1$ , but at a smaller density than photons in models with  $B = 10^{14}$  G. Thus, there is no rotation of the plane of linear polarization at the lower field strength, and the magnitude of the polarization fraction  $|\Pi^{\text{em}}|$  is larger for  $B = 10^{14}$  G.

## 4.2 Observed Stokes Parameters

The observed polarization signals are calculated by multiplying the atmosphere polarization fraction  $\Pi_E^{\text{em}}$  by the angular factors in equations (10) and (11). Thus, the characteristics of intrinsic atmosphere emission are modulated by the projection of the NS magnetic field direction into the  $xy$  plane.

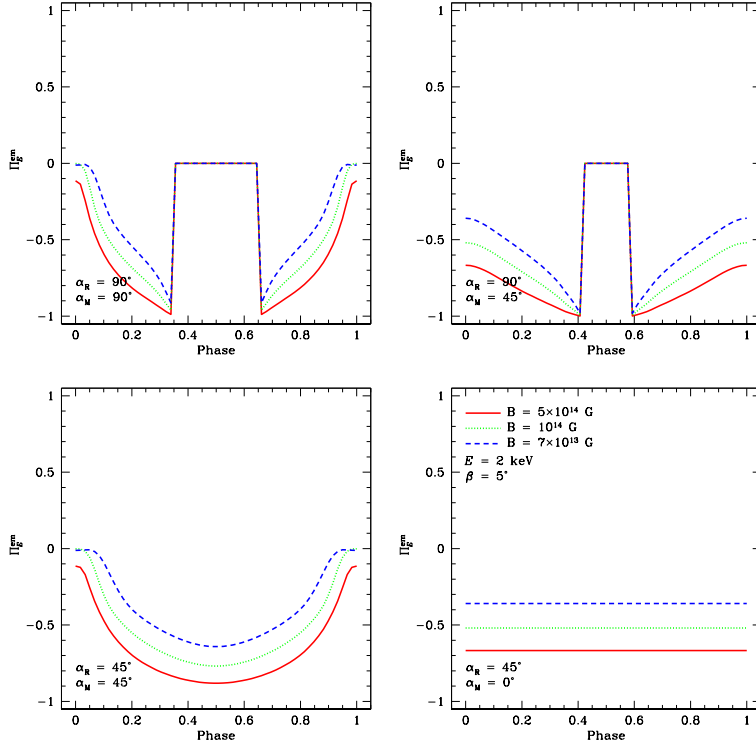


**Figure 2.** Emitted polarization fraction,  $\Pi_E^{\text{em}} \equiv (I_O - I_X)/(I_O + I_X)$ , as a function of phase, for an extended spot on a NS surface. The spot is located at the magnetic pole and has opening angle  $\beta = 5^\circ$ . Results are shown for four NS geometries and three magnetic field strengths:  $B = 5 \times 10^{14}$  G (solid curve),  $B = 10^{14}$  G (dotted curve), and  $B = 7 \times 10^{13}$  G (dashed curve). The angles  $\alpha_R$  and  $\alpha_M$  are the polar inclinations of the rotation axis relative to the line of sight, and the magnetic dipole vector relative to the rotation axis, respectively. The photon energy is set to  $E = 2$  keV.

Figures 3–6 show the observed, normalized photon Stokes parameters  $Q_E/I_E$  (solid curves) and  $U_E/I_E$  (dotted curves) at energies  $E = 0.5$  keV and  $E = 2$  keV as a function of phase, for NS atmospheres with magnetic field strengths  $B = 5 \times 10^{14}$  G (heavy lines) and  $B = 7 \times 10^{13}$  G (light lines). Each panel in the figures corresponds to one of the NS geometries described above. In Figures 3 and 4, the opening angle of the polar cap is set to  $\beta = 5^\circ$ , while in figures 5 and 6 it is set to  $\beta = 30^\circ$ .

In the case of the orthogonal rotator,  $\sin(2\varphi_B) = 0$ , and  $\cos(2\varphi_B) = -1$ , yielding  $Q_E/I_E = -\Pi_E^{\text{em}}$ ,  $U_E/I_E = 0$ . Thus, the projection of the magnetic field into the  $xy$  plane is along the  $y$  axis. In general, the projection of the dipole magnetic field into the  $xy$  plane far from the NS is approximately equal to that of the magnetic dipole vector shifted by  $\pi$  radians ( $\varphi \rightarrow \varphi_B + \pi$ ). It is also important to note that the results are not qualitatively sensitive to the polar cap size; the most significant difference between Figures 3, 4 and 5, 6 are the larger ranges of phase over which the spot is visible.

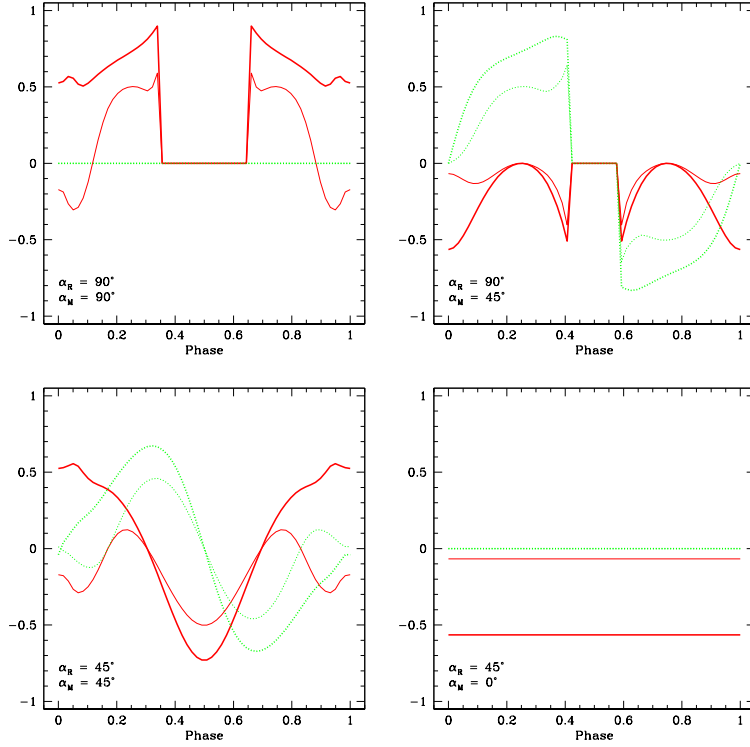


**Figure 3.** Observed, normalized Stokes parameters  $Q/I$  (solid curves),  $U/I$  (dotted curves), as a function of phase, for an extended spot on a NS surface. The spot has opening angle  $\beta = 5^\circ$ . Results are shown for the same geometries as in figure 1, for magnetic field strengths  $B = 5 \times 10^{14}$  G (heavy curves) and  $B = 7 \times 10^{13}$  G (light curves). The photon energy is set to  $E = 0.5$  keV.

### 4.3 Phase-Averaged Polarimetry

A unique signature of vacuum polarization effects on the evolution of photon modes was first reported by Lai & Ho (2003a). For NS with magnetic fields  $B < 7 \times 10^{13}$  G, the vacuum resonance density is less than the decoupling densities of X and O mode photons. Thus, photons which have decoupled from the NS atmosphere undergo partial mode conversion at the vacuum resonance. At low energies,  $E \ll E_{\text{ad}}$ , and  $\Pi_{\text{em}}$  is unaffected. However, at high energies,  $E > E_{\text{ad}}$ , and the sign of  $\Pi_{\text{em}}$  reverses. Thus, there is a rotation of the plane of linear polarization between low and high energy photons.

In practice, this effect depends on the NS geometry (see §4.1). For emission angles  $\delta \approx 0$ ,  $E_{\text{ad}} \approx 0$  and no rotation between low and high photon energies is observed. In geometries for which the typical emission angle is  $\delta \approx \pi/4$ , the effect can be pronounced. Figure 7 shows the phase-averaged Stokes parameter  $Q_{\text{ave}} \equiv (2\pi)^{-1} \int_0^{2\pi} d\psi Q(\psi)$  as a function of photon energy for several magnetic fields with  $B = 4 - 50 \times 10^{13}$  G. The geometry is case G2 with opening angle  $\beta = 5^\circ$ . Note that  $U_{\text{ave}}$  vanishes by symmetry. For  $B = 4 \times 10^{13}$  G (solid curve),  $Q_{\text{ave}}$  changes sign at  $E \approx 1.5$  keV, the energy at which resonant mode conversion

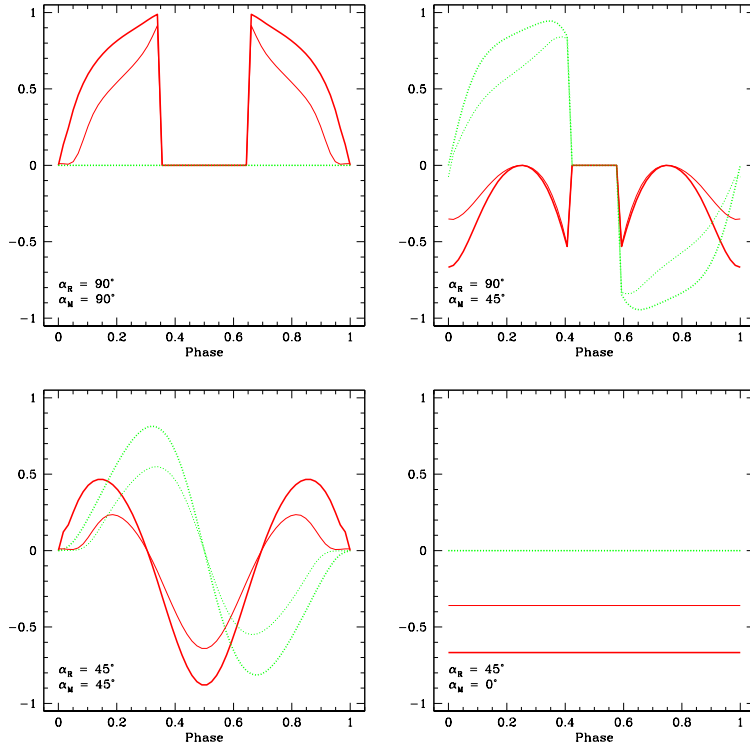


**Figure 4.** Observed, normalized Stokes parameters  $Q/I$  (solid curves),  $U/I$  (dotted curves), as a function of phase, for an extended spot on a NS surface. The spot has opening angle  $\beta = 5^\circ$ . Results are shown for the same geometries as in figure 1, for magnetic field strengths  $B = 5 \times 10^{14}$  G (heavy curves) and  $B = 7 \times 10^{13}$  G (light curves). The photon energy is set to  $E = 2$  keV.

becomes effective. For  $B = 7 \times 10^{13}$  G, the vacuum resonance density is nearly equal to the O mode decoupling density, depending on the NS rotational phase. For most values of  $\psi$ ,  $\rho = \rho_V$  is within the X and O mode photospheres, and no rotation of the plane of polarization occurs. Thus,  $Q_{\text{ave}}$  retains the same sign at low and high energies (c.f., figure 20 of van Adelsberg & Lai 2006, for a similar result in a different geometry).

#### 4.4 Polarization, Atmosphere Composition, and NS Equation of State

Magnetar atmospheres are typically assumed to consist of mostly hydrogen. However, if hydrogen is depleted by thermonuclear burning in the photosphere, they may consist of helium (Chang et al. 2004). For fully ionized helium composition at  $B = 5 \times 10^{14}$  G, and  $T_{\text{eff}} = 5 \times 10^6$  K, we find that the observed Stokes parameters differ from those in the hydrogen case by  $\lesssim 10\%$  for  $0.1 < E < 10$  keV. We therefore do not show results for this case. The reason for the similarity is that the O mode decoupling depth in ionized helium is  $\sim 60\%$  of that in hydrogen, while the vacuum resonance density (identified with the X mode decoupling depth at large magnetic field strengths) increases by a factor of two. The temperature profile evolves much more slowly than the density; in an interval in which the

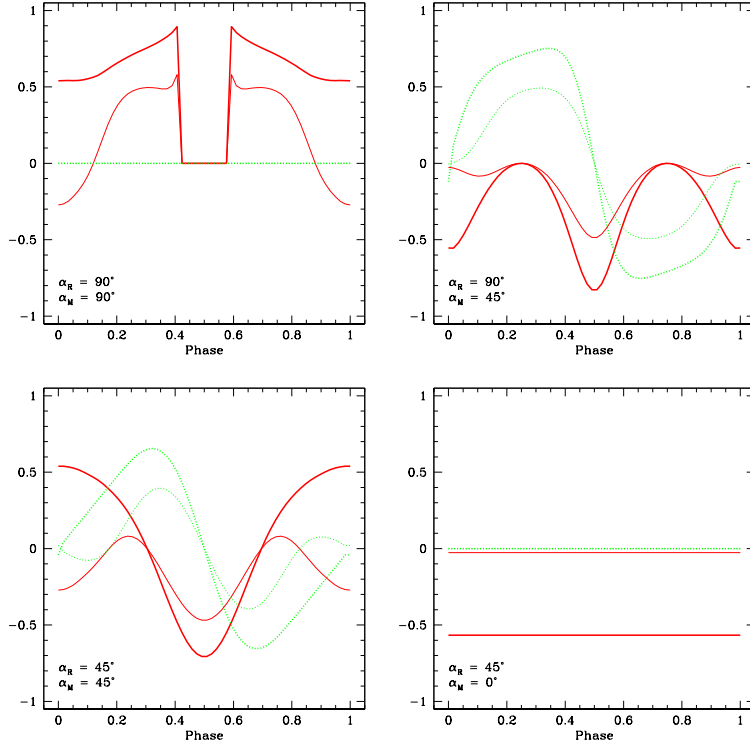


**Figure 5.** Observed, normalized Stokes parameters  $Q/I$  (solid curves),  $U/I$  (dotted curves), as a function of phase, for an extended spot on a NS surface. The spot has opening angle  $\beta = 30^\circ$ . Results are shown for the same geometries as in figure 1, for magnetic field strengths  $B = 5 \times 10^{14}$  G (heavy curves) and  $B = 7 \times 10^{13}$  G (light curves). The photon energy is set to  $E = 0.5$  keV.

density increases by several orders of magnitude, the temperature only changes by a factor of a few. Thus, at most energies and propagation angles, the relative decoupling temperatures of X and O photons are similar to those in the hydrogen case, and we expect to see the same qualitative features, with a slightly larger magnitude of the helium polarization fraction. Nevertheless, at lower fields, the reduction of the O mode decoupling depth and increase in the resonance density suppresses the rotation of the plane of polarization between low and high energy photons at  $B \approx 4 \times 10^{13}$  G. For helium, lower magnetic fields, which are unlikely to occur in the magnetar regime, are necessary to see this effect.

We also explored the dependence of the emitted polarization fraction on the equation of state of the star. In particular, for the case of  $B = 5 \times 10^{14}$  G and  $\beta = 5^\circ$ , we compared the polarization fraction for three values of the NS radius,  $R = 9, 12, 15$  km with the NS mass fixed at  $M = 1.4M_\odot$ . For the four geometries defined above, we found that the range of  $\psi$  for which the spot is visible increases with decreasing radius. This result is expected, due to light deflection effects around relativistic stars. However, the difference between the emitted polarization fraction for the two extreme radii is  $|\Pi_E^{\text{em}}(R = 15 \text{ km}) - \Pi_E^{\text{em}}(R = 9 \text{ km})|/|\Pi_E^{\text{em}}(R = 15 \text{ km})| \ll 1$ , for most values of  $\psi$ . Since the phased flux modulation of

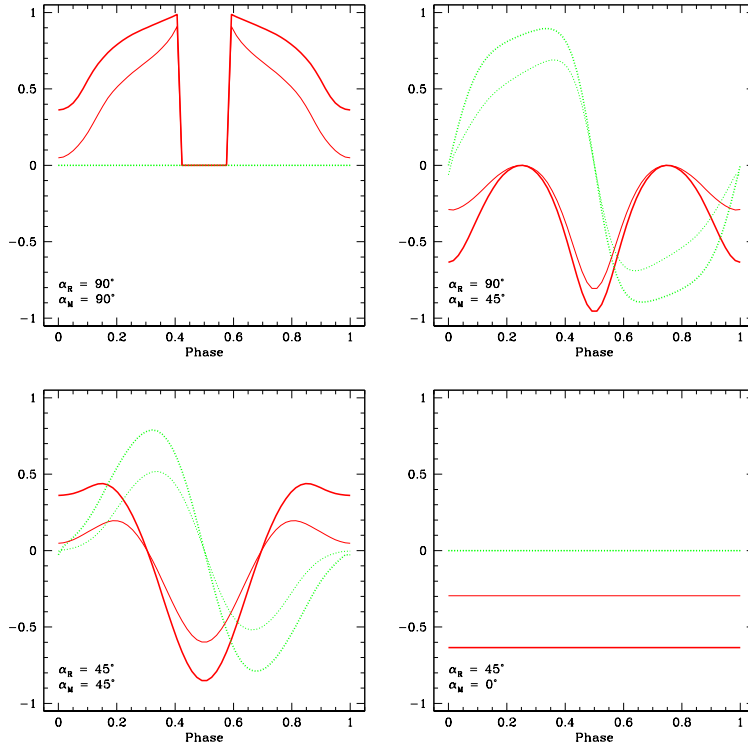


**Figure 6.** Observed, normalized Stokes parameters  $Q/I$  (solid curves),  $U/I$  (dotted curves), as a function of phase, for an extended spot on a NS surface. The spot has opening angle  $\beta = 30^\circ$ . Results are shown for the same geometries as in figure 1, for magnetic field strengths  $B = 5 \times 10^{14}$  G (heavy curves) and  $B = 7 \times 10^{13}$  G (light curves). The photon energy is set to  $E = 2$  keV.

the X and O mode photons is equally affected by changes in the NS radius, the variation in the linear polarization fraction with  $R$  is associated with two effects that vary with NS compactness: (1) the difference between the energy at the star surface and the observed energy, and (2) the range of emission angles  $\delta$  for which photons reach the observer at a given rotational phase  $\psi$ . The ratio of emitted energies corresponding to the same observed energy for stars with  $R = 9$  km and  $R = 15$  km is  $E_9/E_{15} \approx 1.15$ . Similarly, the difference in the range of  $\delta$  for photons which reach the observer, at a given  $\theta$ , is smaller than the spot size for small  $\theta$ , and, for most geometries, is generally smaller than the range over which substantial polarization variations occur. Therefore, the polarization signal has no significant, direct dependence on the EOS of the NS.

## 5 DISCUSSION

Current studies of NSs rely on spectroscopy to constrain the stars' physical parameters. Fits to the phase-averaged X-ray spectrum yield the effective temperature of the star and the size of the emitting region, but are insensitive to the viewing geometry. Timing analysis

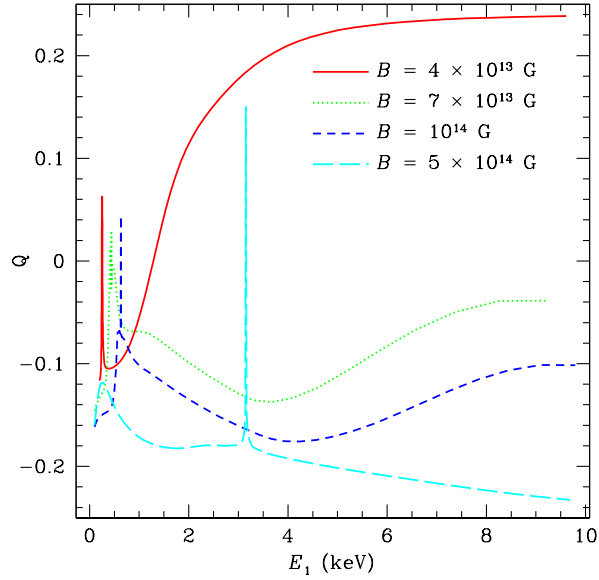


**Figure 7.** Phase-averaged Stokes parameter  $Q$  as a function of photon energy  $E$  (keV).

complements the information obtained from spectral fits by constraining the permitted values of  $\alpha_R$  and  $\alpha_M$ . However, since the amplitude of the modulation of the flux with phase is largely dependent on the mass-to-radius ratio of the star, there is a degeneracy between the inferred viewing geometry and compactness ratio (e.g., Perna & Gotthelf 2008).

As shown above, our calculations of the magnetar polarization signal are not sensitive to  $M/R$ , and can therefore be used to break this degeneracy. Moreover, the sensitivity of the Stokes parameters to the magnetic field strength can be used to constrain the magnetar magnetic field. In particular, the phase-averaged behavior of the Stokes parameters at low and high photon energies in the soft X-ray band can put lower or upper limits on  $B$  (in the absence or presence of rotation of the plane of linear polarization, respectively).

Measurements of the magnetic field of a magnetar from the shape of the continuum X-ray spectrum alone are extremely difficult to perform. Magnetic atmosphere models are characterized by hard tails with respect to blackbody emission (this discrepancy is larger for magnetic fields  $B < B_Q$ ; see Ho & Lai 2003; van Adelsberg & Lai 2006). Spectral fits are generally unable to uniquely discriminate among different B-field strengths based on the spectral shape alone, especially since hard tails are also predicted from scattering in the atmosphere (Rea et al. 2008). While no features have been detected in quiescent magnetar thermal spectra, there is one confirmed detection of an absorption-like feature in an outburst of the Anomalous X-ray Pulsar 1XRSJ170849-400910 (Rea et al. 2003). The phase-dependent feature occurs at 8.1 keV in the magnetar spectrum, consistent with res-

onant cyclotron scattering by electrons at  $9 \times 10^{11}$  G or ions at  $1.6 \times 10^{15}$  G. The value of the magnetic field inferred from dipole spin-down is  $B \sim 5 \times 10^{14}$  G, however, much higher surface fields are possible if the magnetic field is dominated there by higher-order multipoles. Nevertheless, an unambiguous identification of the line feature, and hence, magnetic field strength, is not possible. Future measurements of Stokes parameters in the soft X-ray band may help break this degeneracy. If the rotation of the plane of linear polarization is not observed, this is consistent with a the magnetar in the strong magnetic field regime, and the identification of the line feature with ion cyclotron resonance becomes more certain.

## ACKNOWLEDGEMENTS

We thank Tim Kallman for motivating this work, and Dong Lai for very useful comments on the manuscript.

## REFERENCES

- Becker, W., & Pavlov, G. G. 2002, in *The Century of Space Science* (Kluwer Academic Publishing), 721–758
- Beloborodov, A. M. 2002, *ApJ*, 566, L85
- Camilo, F., Kaspi, V. M., Lyne, A. G., Manchester, R. N., Bell, J. F., D’Amico, N., McKay, N. P. F., & Crawford, F. 2000, *ApJ*, 541, 367
- Camilo, F., Ransom, S. M., Halpern, J. P., & Reynolds, J. 2007, *ApJ*, 666, L93
- Chang, P., Arras, P., & Bildsten, L. 2004, *ApJ*, 616, L147
- Costa, E., Bellazzini, R., Soffitta, P., Muleri, F., Feroci, M., Frutti, M., Mastropietro, M., Pacciani, L., Rubini, A., Morelli, E., Baldini, L., Bitti, F., Brez, A., Cavalca, F., Latronico, L., Massai, M. M., Omodei, N., Pinchera, M., Sgró, C., Spandre, G., Matt, G., Perola, G. C., Chincarini, G., Citterio, O., Tagliaferri, G., Pareschi, G., & Cotroneo, V. 2006, in *Society of Photo-Optical Instrumentation Engineers (SPIE) Conference Series*, Vol. 6266, *Society of Photo-Optical Instrumentation Engineers (SPIE) Conference Series*
- Costa, E., Soffitta, P., Bellazzini, R., Brez, A., Lumb, N., & Spandre, G. 2001, *Nature*, 411, 662
- De Luca, A., Caraveo, P. A., Mereghetti, S., Negroni, M., & Bignami, G. F. 2005, *ApJ*, 623, 1051
- Fernández, R., & Thompson, C. 2007, *ApJ*, 660, 615

- Gonzalez, M. E., Kaspi, V. M., Lyne, A. G., & Pivovarov, M. J. 2004, *ApJ*, 610, L37
- Haberl, F. 2007, *Ap&SS*, 308, 181
- Heyl, J. S., & Shaviv, N. J. 2000, *MNRAS*, 311, 555
- . 2002, *Phys. Rev. D*, 66, 023002
- Heyl, J. S., Shaviv, N. J., & Lloyd, D. 2003, *MNRAS*, 342, 134
- Ho, W. C. G., & Lai, D. 2001, *MNRAS*, 327, 1081
- . 2003, *MNRAS*, 338, 233
- Ho, W. C. G., Lai, D., Potekhin, A. Y., & Chabrier, G. 2003, *ApJ*, 599, 1293
- Israel, G. L., Campana, S., Dall’Osso, S., Munro, M. P., Cummings, J., Perna, R., & Stella, L. 2007, *ApJ*, 664, 448
- Kallman, T. 2004, *Advances in Space Research*, 34, 2673
- Kargaltsev, O. Y., Pavlov, G. G., Zavlin, V. E., & Romani, R. W. 2005, *ApJ*, 625, 307
- Kaspi, V. M. 2004, in *IAU Symposium, Vol. 218, Young Neutron Stars and Their Environments*, ed. F. Camilo & B. M. Gaensler, 231–+
- Kaspi, V. M., & McLaughlin, M. A. 2005, *ApJ*, 618, L41
- Kulkarni, S. R., Kaplan, D. L., Marshall, H. L., Frail, D. A., Murakami, T., & Yonetoku, D. 2003, *ApJ*, 585, 948
- Lai, D., & Ho, W. C. 2003a, *Physical Review Letters*, 91, 071101
- Lai, D., & Ho, W. C. G. 2002, *ApJ*, 566, 373
- . 2003b, *ApJ*, 588, 962
- Livingstone, M. A., Kaspi, V. M., Gotthelf, E. V., & Kuiper, L. 2006, *ApJ*, 647, 1286
- Lyutikov, M., & Gavriil, F. P. 2006, *MNRAS*, 368, 690
- Marshall, H. L., & Schulz, N. S. 2002, *ApJ*, 574, 377
- Medin, Z., & Lai, D. 2006, *Phys. Rev. A*, 74, 062508
- Mereghetti, S., Tiengo, A., Esposito, P., Götz, D., Stella, L., Israel, G. L., Rea, N., Feroci, M., Turolla, R., & Zane, S. 2005, *ApJ*, 628, 938
- Meszaros, P. 1992, *High-energy radiation from magnetized neutron stars (Theoretical Astrophysics)*, Chicago: University of Chicago Press, —c1992)
- Mori, K., Chonko, J. C., & Hailey, C. J. 2005, *ApJ*, 631, 1082
- Novick, R., Weisskopf, M. C., Berthelsdorf, R., Linke, R., & Wolff, R. S. 1972, *ApJ*, 174, L1+
- Page, D. 1995, *ApJ*, 442, 273
- Pavlov, G. G., Shibano, Y. A., Ventura, J., & Zavlin, V. E. 1994, *A&A*, 289, 837

- Pechenick, K. R., Ftaclas, C., & Cohen, J. M. 1983, *ApJ*, 274, 846
- Perna, R., & Gotthelf, E. V. 2008, *ApJ*, 681, 522
- Prakash, M., Lattimer, J. M., Pons, J. A., Steiner, A. W., & Reddy, S. 2001, in *Lecture Notes in Physics*, Berlin Springer Verlag, Vol. 578, *Physics of Neutron Star Interiors*, ed. D. Blaschke, N. K. Glendenning, & A. Sedrakian, 364–+
- Rea, N., Israel, G. L., Stella, L., Oosterbroek, T., Mereghetti, S., Angelini, L., Campana, S., & Covino, S. 2003, *ApJ*, 586, L65
- Rea, N., Zane, S., Turolla, R., Lyutikov, M., & Götz, D. 2008, *ApJ*, 686, 1245
- Sanwal, D., Pavlov, G. G., Zavlin, V. E., & Teter, M. A. 2002, *ApJ*, 574, L61
- Shapiro, S. L., & Teukolsky, S. A. 1986, *Black Holes, White Dwarfs and Neutron Stars: The Physics of Compact Objects (Black Holes, White Dwarfs and Neutron Stars: The Physics of Compact Objects, by Stuart L. Shapiro, Saul A. Teukolsky, pp. 672. ISBN 0-471-87316-0. Wiley-VCH , June 1986.)*
- Thompson, C., Lyutikov, M., & Kulkarni, S. R. 2002, *ApJ*, 574, 332
- Tiengo, A., Mereghetti, S., Turolla, R., Zane, S., Rea, N., Stella, L., & Israel, G. L. 2005, *A&A*, 437, 997
- van Adelsberg, M., & Lai, D. 2006, *MNRAS*, 373, 1495
- van Adelsberg, M., Lai, D., Potekhin, A. Y., & Arras, P. 2005, *ApJ*, 628, 902
- Wang, C., & Lai, D. 2009, *astro-ph/0903.2094*
- Weisskopf, M. C., Cohen, G. G., Kestenbaum, H. L., Long, K. S., Novick, R., & Wolff, R. S. 1976, *ApJ*, 208, L125
- Woods, P. M., & Thompson, C. 2006, *Soft gamma repeaters and anomalous X-ray pulsars: magnetar candidates (Compact stellar X-ray sources)*, 547–586
- Yakovlev, D. G., & Pethick, C. J. 2004, *ARA&A*, 42, 169